Solar Phys (2012) 280:205–221
DOI 10.1007/s11207-012-0043-4

A Comparison of the 10.7-cm Radio Flux Values and the International Sunspot Numbers for Solar Activity Cycles 19, 20, and 21

Robert A. Greenkorn

Received: 9 June 2010 / Accepted: 24 May 2012 / Published online: 17 July 2012

Abstract A nonlinear analysis of the daily 10.7-cm radio flux values for each of Solar Cycles 19, 20, and 21 is used to determine if the results match those of the International Sunspot Numbers for each of these cycles. Fractals and chaos are described and a brief review of utilizing fractals and chaos is given. The origin of the 10.7-cm radio flux is discussed and a short review of recent work discussing its measurement and its relation to the international sunspot number and other proxies for solar activity cycles given. The parameters used to describe chaos for the 10.7-cm radio flux are discussed. The length of the data sets for either statistical analysis or nonlinear analysis of the 10.7-cm radio flux values is considered. These results indicate that the 10.7-cm radio flux values appear to be stochastic for Cycle 19 and chaotic for Cycles 20 and 21. The International Sunspot Numbers show similar behavior for these three cycles. A day-by-day comparison of the dimensionless 10.7-cm radio flux values and the dimensionless International Sunspot Numbers differences shows a linear trend. The results remain consistent in that the 10.7-cm radio flux values indicate, as did the International Sunspot Numbers, that there is a transition from stochastic behavior for Cycle 19 to chaotic behavior in Cycles 20 and 21. The day-by-day comparison of the 10.7-cm radio flux values and the International Sunspot Numbers emphasizes that the 10.7 cm radio flux values are responding to the magnetic field associated with the sunspots.

Keywords Radio flux · Sunspots · Activity cycles · Chaos

1. Introduction

A goal of observing solar phenomena is to understand how solar activity occurs. The objective of this study is to compare the 10.7-cm radio flux values [$F_{10.7}$] with the International Sunspot Numbers [R_i] for solar-activity Cycles 19, 20, and 21.

Electronic supplementary material The online version of this article (doi:10.1007/s11207-012-0043-4) contains supplementary material, which is available to authorized users.

R.A. Greenkorn (✉)
School of Chemical Engineering, Purdue University, West Lafayette, IN, USA
e-mail: greenkor@ecn.purdue.edu

The Sun's magnetic field appears concentrated in flux tubes or ropes that appear on the surface of the photosphere as sunspots, pores, plages, and surface network. The magnetic fields that result from the solar dynamo include all solar motions (Ruzmakin, 2001; Rogachevskii and Kleeorin, 2007). R_i and $F_{10.7}$ are proxies for phenomena associated with the solar cycle (Eddy, 1977).

The International Sunspot Number [R_i] is the weighted sum of the number of spots and spot groups on the solar disk at one time:

$$R_i = k(10g + f), \tag{1}$$

where f is the total number of spots on the visible disk irrespective of size, g is the number of spot groups, k is a coefficient depending on the observer's method of counting and subdividing them into groups, the size of the telescope, the magnification, and seeing conditions. The index R_i is not the number of spots but a relative number including groups. The sunspot number usually reaches a maximum three or four years after the start of a solar-activity cycle and declines for seven or eight years. Thus the average activity cycle lasts about eleven years. Sunspots are a convenient index for most activity related to the Sun's magnetic fields (Eddy, 1977).

Chaos is described and a brief review of articles utilizing chaos and fractals are presented. Another measure of solar activity is the 10.7-cm radio flux values [$F_{10.7}$]. The flux results from thermal ionization at the photosphere–chromosphere interface and from magnetic resonance above sunspots and plages (Tapping and DeTracy, 1990). The origin of the 10.7-cm radio flux is discussed and a short review of recent work discussing its measurement and its relation to the International Sunspot Number and other proxies for solar-activity cycles. One would expect R_i and $F_{10.7}$ to be correlated.

Synoptic radio observations of the Sun were started in Canada in November 1946 and became an observing program of $F_{10.7}$ in 1947 (Covington, 1948). The values are reported in solar flux units [sfu $= 10^{-22}$ W $(\mathrm{m}^2\,\mathrm{Hz})^{-1}$]. $F_{10.7}$ is used as a proxy for R_i, sunspot area, E-Layer ionization index, Lyman β, Mg II, EU, EUV, and total irradiance (Schmahl and Kundu, 1998).

Section 2 presents a brief discussion of fractals and chaos applied to R_i and $F_{10.7}$.

Section 3 presents the origin of the 10.7-cm radio flux values and includes a brief review of articles that discuss measurement of the radio flux and its relation to the International Sunspot Numbers and other proxies for solar activity. The relation between the proxies is discussed including chaos. Differences, time scales, and fractals are discussed. The use of $F_{10.7}$ in prediction models for activity-cycle properties is examined. Section 4 presents a short history of solar-activity cycles as measured by the sunspot index. Section 5 considers the length of the data sets necessary to analyze the data from a statistical or a nonlinear point of view. Section 6 applies nonlinear analysis to $F_{10.7}$ for Cycles 19, 20, and 21. $F_{10.7}$ for Cycle 19 appears to be stochastic. $F_{10.7}$ for Cycles 20 and 21 appear to be chaotic. Section 7 contains a discussion of the results including a day-by-day comparison of $F_{10.7}$ with R_i. Section 8 presents the conclusions.

2. Fractals and Chaos

A fractal line is not differentiable and is scale independent. A magnified segment resembles the large-scale appearance. The length of a fractal line does not approach a finite limit as the resolution increases but it increases without limit. A familiar example of a complex

line is a coastline (Feder, 1989). To measure the length $[L]$ of a complex line segment such as a coastline, select a measure of length $[\delta]$ and measure along the line segment and obtain the number $[N(\delta)]$ of measures $[\delta]$ to cover the line. The length $[L]$ is the number of measures times the length of the measure, so $L(\delta) = N(\delta) \times \delta$. As the measure δ is decreased, the number of steps $[N]$ required to cover the coast line increases. The measured length increases as δ is reduced. Plotting the length as a function of δ yields a straight line approximated by

$$L(\delta) = a\delta^{1-D}. \tag{2}$$

For an ordinary line, $a = L_{\mathrm{N}}$ and $D = 1$. However for the coast line $D \approx 1.52$, thus the coast line is a fractal with fractal dimension D. A fractal curve (coast line) is a shape made up of parts similar to the whole. A fractal appears the same regardless of scale.

The set of points that make up a line in ordinary Euclidean space has a topological dimension $D_{\mathrm{T}} = 1$. The Euclidean dimension of space is $E = 3$. The set of points that form a surface in $E = 3$ has a topological dimension $D = 2$ and $D_{\mathrm{T}} = 2$. For a sphere, $D = 3$ and $D_{\mathrm{T}} = 3$. Analytically in the limit of small δ

$$N(\delta) \approx 1/\delta^{D}. \tag{3}$$

The fractal dimension of a coast line can be found from the slope of $\ln N(\delta)$ plotted as a function of $\ln \delta$. The fractal dimension of a coast line is 1.52. A fractal looks the same, whatever the scale; it is self-similar.

Chaos is an irregular deterministic motion characterized by a continuous, broad-band Fourier power spectrum in a three or higher dimension nonlinear system. Chaos occurs between regular behavior and stochastic behavior. An attractor is a point or set of points in phase space towards which a system evolves over time. Systems with low dissipation could take a very long time. An attractor can have a regular dimension – a regular attractor, or a fractal dimension – a strange attractor.

The stability of motions on an attractor is determined by the Lyapunov exponents. The stability can be determined from the Jacobian matrix of the dynamics. The eigenvalues of the matrix are determined (Oseledec, 1968). The eigenvalues are $\mathrm{e}^{\lambda_1}, \mathrm{e}^{\lambda_2}, \ldots, \mathrm{e}^{\lambda_a}$, where $\lambda_1 \geq \lambda_2 \geq \cdots \geq \lambda_d$ are the global Lyapunov exponents.

Measurements such as daily values of the sunspot number or the 10.7-cm radio flux result in a time sequence sampled at intervals of τ initiated at t_0.

$$s(t) = s(t_0 + n\tau) = s(n). \tag{4}$$

Chaos has structure in phase space. Time-lagged variables are the coordinates for a phase space in d_{E} dimensions,

$$\boldsymbol{y}(n) = \big[s(n), s(n+T), \ldots, s\big(n + (d_{\mathrm{E}} - 1)T\big)\big], \tag{5}$$

where T is time lag and d_{E} is embedding dimension. The global embedding dimension is the lowest dimension that unfolds the attractor (the set of points visited by a signal trajectory) so that there are no overlaps from projection of the attractor to a lower dimension. The embedding theorem (Takens, 1980) is: If the dimension of the attractor defined by the orbits is d_{A} the attractor will unfold in an integer-dimensional space of dimension d_{E}, where $d_{\mathrm{E}} \geq 2d_{\mathrm{A}}$.

The two invariants of the motion are the fractal dimension of the attractor and the Lyapunov exponents. The correlation dimension $[D_2]$ is a fractal dimension associated with an

inhomogeneous attractor that quantifies self-similarity. The slope of the correlation function is D_2 (Grassberger and Procaccia, 1983). Although the correlation dimension [D_2] applies to the attractor, the existence of a scaling region does not necessarily indicate that the data are chaotic. Stochastic data may also have a scaling region.

3. Review

The topics reviewed in this section are: the origin of the 10.7-cm radio flux; solar activity; the relations between proxies for the activity cycles, differences, time scales, and fractals.

3.1. The 10.7-cm Radio Flux Values $F_{10.7}$

The integrated emission of centimeter wavelengths from the whole solar disk is separated into three components based on characteristic time scales: transient events such as flares with durations less than an hour; slow variation over hours to years; a continuous minimum level, the quiet-Sun level. The second component with time scales of hours to years is called the S-component (Tapping and DeTracy, 1990).

The S-component at 10.7-cm wavelength has been measured since 1947 (Covington, 1947). $F_{10.7}$ is a measure of solar activity and is a proxy for other measures such as: the sunspot index (Covington, 1948); the full-disk flux in Ca II and Mg II (Donnelly, 1987); the integrated fluxes in ultraviolet (UV) and in extreme ultraviolet (EUV) (Schmahl and Kundu, 1998). When the full-disk X-ray flux activity is high, $F_{10.7}$ and the X-ray flux are correlated (Tapping and DeTracy, 1990).

The intensities of the Ca II and Mg II spectral lines are functions of chromospheric density and temperature. X-rays are produced in the corona. The S-component is integrated emission from all sources on the solar disk with contributions from thermal free–free and gyroresonant processes, and some non-thermal emissions. The relative magnitude of these mechanisms is a function of wavelength and time (Tapping and DeTracy, 1990). The spatial distribution of the two thermal mechanisms are different. The gyroresonant emission is mainly in the vicinity of sunspots where magnetic fields are strong. Free–free emission is more widely distributed.

The correlation of $F_{10.7}$ and R_i implies a connection with strong magnetic fields. The correlation of $F_{10.7}$ with other phenomena (Ca II, Mg II, UV, EUV, and X-rays) implies a relation with widely distributed phenomena. Gyroresonance requires strong magnetic-field strengths, which occur in the vicinity of sunspots. Free–free emissions take place over the entire solar disk – the quiet Sun level (64 sfu) – with enhanced emission produced where the densities in the chromosphere and corona are above the usual values. A value of $F_{10.7}$ is apparently an indication of the density in the low corona.

Tapping and DeTracy (1990) construct a two component model: an isothermal chromosphere at $T = 10^4$ K and a homogeneous corona at $T = 10^6$ K. Variations of the thickness of the chromosphere, transition region, and mixed zone cause only small changes in the S-component spectrum of the model. There is a strong dependence on plasma density at the base of the corona. Dependence on a few quantities and its origin in the low corona makes it useful as an index of solar activity.

Total-irradiance variation may affect the Earth's climate. To understand the role of irradiance variation requires a long record. Proxies and/or models are used to generate long records. Most models are based on the assumption of two irradiance variations which may vary with time: the cyclic component that follows R_i and $F_{10.7}$, and a secular component, the

quiet Sun, with variations on time scales much longer than a solar-activity cycle. Extending such models back in time to the Maunder minimum allows one to estimate the secular component at that time. Extrapolations in time assume that the relationship between indices used in the models do not change. Short-term irradiance variation correlates with bright faculae and magnetic networks (Tapping *et al.*, 2007).

The input to the models is R_i and $F_{10.7}$. There are two approaches to modeling irradiance. One approach assumes that irradiance is a photospheric mechanism (Foukal and Lean, 1990). The other approach uses more global variation due to small temperature changes in the photospheric temperature outside active regions. This approach may involve change in the photospheric radius (Ulrich and Bertello, 1995).

Rotation of the Sun's atmosphere is affected by the magnetic structure in the convection zone. Sunspots have been used to determine rotation rates. Changes in the size of the convection-zone radius may be due to changes in the turbulence regime in the convection zone (Greenkorn, 2009). $F_{10.7}$ can also be used to determine rotation rates. Sunspot measurements provide differential-rotation rates over long periods. Data from the analysis of the $F_{10.7}$ flux measurements are frequency distributed with respect to time. There are regions on the Sun with rigid and differential-rotation properties in both the photosphere and the corona (Mouradian, Bocchia, and Botton, 2002).

3.2. Solar Activity

$F_{10.7}$ is an indicator of radiative variability. The $F_{10.7}$ flux is the basis for estimating radiative output when no absolute measurements are available (White and Rottman, 2000). Radio observations are used to study the solar atmosphere. They can be used to probe the chromosphere up to the middle of the corona. Radio observations provide information about the magnetic field. Where the magnetic fields are strong, strong emissions can be produced at low harmonics of the electron gyrofrequency. This thermal-electron gyroresonance is bright, narrowband, and highly polarized. This emission is associated with the strong magnetic fields over sunspots (Alissandrakis, 1997). In the chromosphere and corona above active regions, the magnetic fields are too weak for gyroresonance. Emission is produced by thermal free–free processes. Polarization is introduced by propagation through the plasma giving additional information about the magnetic field. The beginning of a new activity cycle is the transition from a quiet Sun to an active Sun with a complex magnetic atmosphere. Active longitudes contain sunspot nests. Solar minimum is a time mark in statistical schemes for predicting solar activity. R_i, $F_{10.7}$, and the Mg II index follow the increase in the observed magnetic field (DeToma, White, and Harvey, 2000).

Solar-activity indices show variation from a few days to several years. The most prominent short-term variation is the 27-day periodicity due to solar rotation. Sunspots and magnetic features rotate faster than the solar plasma, probably due to magnetic linkage to faster rotating sub-surface layers (Howard, 1984) or due to buoyancy and drag coupled with Coriolis force (D'Silva and Howard, 1994). Bouwer, Pap, and Donnelly (1990) report that magnetic and photospheric rotation is at a period of 25 days, Mg II and $F_{10.7}$ at 27 days, and coronal X-rays at 28 days. Spectral analysis of the time series of 10.7-cm solar radio emissions [$F_{10.7}$] and R_i show periodicities in the range of 11 to 70 days, which could be due to a combination of active-region durations, the number of complexes or active longitudes, and solar rotation. Group sunspot numbers correlate with the 10.7-cm flux but not as well as with the sunspot index (Kane, Vats, and Sawant, 2001). This higher correlation with groups may be due to a significant part of the $F_{10.7}$ originating over an active region beyond a sunspot. A group of sunspots is more likely to be associated with a large area of plage over which free–free emission is produced.

3.3. Relation of $F_{10.7}$ with Other Proxies

$F_{10.7}$ is a single-wavelength measurement of the S-component made close to the spectral peak. Solar soft X-rays and $F_{10.7}$ are highly correlated, probably because they both are produced in the solar corona, where the electron temperature exceeds a million Kelvin. The solar soft X-rays and the slowly varying component of the 10.7-cm radio flux are emitted from the solar corona where $T \geq 10^6$ K and they are correlated. $F_{10.7}$ is used in atmospheric and ionospheric models as an indicator of solar activity of the UV and EUV radiations (Donnelly, 1982; Chatterjee and Das, 1995). A statistical analysis of the relation between $F_{10.7}$ and R_i on a daily basis showed the correlation between them is very high (Xanthakis and Poulakos, 1985). Empirical relationships for the calculation of monthly and annual indices of the radio flux and sunspot numbers are available (Kononovich, Shefov, and Khramova, 2002). There is also a correlation of the radio flux with plage area (Oster, 1990). Despite the strong correlation, the two indices behave differently at solar-activity-cycle maximum. This could be due to a change in the way that magnetic activity is manifested over a solar cycle (Wilson, Rabin, and Moore, 1987), such as differences in the ratio of spot area to plage area. Change in the area ratio would change the relative contribution to $F_{10.7}$ by gyroresonance and free–free emissions, such as changes in the relative contributions of gyroresonance and free–free emission over the solar cycle.

Global indices of solar activity in terms of nonlinear dynamics show that solar periodicity is a complex dynamic system that may be stochastic at times and chaotic at times. Nonlinear interaction occurs but not between all indices (Salakhutdinova, 1999). Rigozo *et al.* (2001) used a reconstructed sunspot-number series to infer past $F_{10.7}$, solar-wind velocity, and the southward component of the interplanetary magnetic field.

3.4. Differences; Time Scales; and Fractals

In any given active region, the sunspot area usually peaks before the plage area and plage is still present after all sunspots have disappeared. Thus the region's contribution to sunspot related indices, *e.g.* sunspot number, peaks before the contributions to plage-related indices, *e.g.* UV flux and Ca II K index. The $F_{10.7}$ solar radio-flux index is more complex because it contains both spot and plage-related contributions. Bright cores of thermal gyroresonance lie over sunspots, and a diffuse cloud of free–free emission overlies the plage. The brightness temperature of the thermal gyroresonance is higher, but the free–free emission comes from a larger area. The result is that the variation with time of the contribution to the $F_{10.7}$ index can be multi-peaked and can be complicated. The situation may become more complicated by additional magnetic-flux emergence (Donnelly *et al.*, 1983). This complexity affects the correlation of $F_{10.7}$ with the UV flux and of heating and photodissociation of O_2 in the stratosphere and mesosphere. Although the radio flux and sunspot index are well correlated, the temporal variation of the radio flux and sunspot index and Ca K plage data are not as well correlated. The UV flux has a 13-day temporal structure. The radio flux and sunspot index do not show the 13-day temporal structure. They do have a broader dependence on the solar central meridian distance (CMD). The CMD-dependence of cm-wavelength emission of active regions differs from the effective-area foreshortening of plages because coronal radio emissions are moderately strong from active regions at the solar limb. Another type of difference in the temporal variation occurs during the evolution of major active regions that dominate the full disk. Simple regression estimates of UV flux based on radio-flux values or sunspot numbers fail to fit the temporal variation of the UV flux. Plages are usually lasting longer than sunspots associated with the same active regions. R_i peaks earlier than

UV because major active regions of sunspot activity peak earlier than plage activity. Part of the radio-flux emissions are from small intense cores in regions of strong coronal magnetic fields and gyroresonant emissions from active regions tend to peak earlier and decay more rapidly than associated UV plage emissions. Radio emissions from solar active regions are complicated. The radio flux peaks and decays more rapidly than plage emissions and behaves more like sunspot evolution. Although there are some similarities among the time scales of UV fluxes, radio-flux emissions, and sunspot numbers on rotation and evolution, there are differences. Strong 13-day modulation lasting months occurs. There are differences due to CMD dependence. Simple linear regression estimates of UV flux based on R_i and $F_{10.7}$ fail to fit the temporal variation of the UV flux (Donnelly *et al.*, 1983).

The green coronal brightness indices [CI: Fe XIV, $\lambda = 530.3$ nm] in the minima of Cycles 19 – 20, 20 – 21, and 21 – 22 were compared with R_i and $F_{10.7}$ for 1964 – 1987. The patterns of the three are similar. The minimum between Cycles 21 – 22 is different from that between the two previous minima. The most significant changes were in CI, which may be a better proxy to study the Sun (Rušin and Rybansky, 1990).

Fractals were used to examine R_i (1854 – 1996), total sunspot area (1874 – 1983), $F_{10.7}$ (1964 – 1996), and Stanford mean magnetic field (1975 – 1996) (Salakhutdinova, 1998). Similar values of the fractal dimensions of these indices on different time scales were determined. For sunspot numbers, total sunspot area, and radio flux there are three time scales: two days – two months, two months – two years, and $>$ two years with values of fractal dimensions of 1.5, 2, 1.2 – 1.6 respectively.

Fractals are used to examine R_i, $F_{10.7}$, Ly α, Fe XIV, and total solar irradiance (Watari, 1995). The fractal dimension approaches two if the time series is random and becomes one for a regular time series. The length of the curve for a time interval k is the average value over sets of $L_m(k)$. If $L(k) \sim k^{-D}$, the curve is fractal with dimension D. The plot of $L(k)$ may have one or more straight-line sections. The straight lines are joined at a point where the slope changes: the bending point. The fractal dimension of the 10.7-cm radio flux in Cycle 21 for periods of $\approx$ seven days or less was 1.28; for periods longer than 272 days was 1.3, and for the interval between them was 1.86. Fractal dimensions for the other indices were similar. For both short and long time scales, the bending points for the radio flux and the sunspot numbers are similar. Two fractal dimensions and one bending point can be found for the daily indices and three fractal dimensions and two bending points can be found for a cycle. The variations of fractal dimensions and bending points for CI are different from the radio flux and sunspot numbers. Fractal dimensions for the sunspot numbers are ≈ 1.5 for both short and long periods. Solar activity is irregular for the time scales between several days and several months. The fractal dimensions for long time scales may reflect a long-term variation due to large solar-scale features. Yearly values of D and bending points of $\langle L(k) \rangle$ do not change with solar cycle.

Watari (1996) calculated the fractal dimensions of the solar radio fluxes for 1976 – 1990 for nine values, ranging from 245 to 15 400 MHz. The fractal values determined were 1.2 – 2.0 for $\leq$ ten days, one – ten months, and $\geq$ ten months. The quiet-Sun emission at different frequencies contains information about densities and temperature in different levels of the solar atmosphere. The strength of the solar radio emission, the S-component, varies with the 11-year solar cycle. The plage-associated emission dominates around 1 – 2 GHz and sunspot-associated emission dominates around 5 GHz. Both the chromosphere and corona contribute to the quiet-Sun emission at decimeter wavelengths. The fractal dimensions of the sunspot number and solar radio flux around 3 GHz show similar behavior, confirming the existence of a close relation between R_i and the radio flux at 2.8 GHz (10.7-cm flux). The quiet-Sun emission at different frequencies contains information about densities and temperature in different layers of the solar atmosphere.

4. Solar Activity Cycles

Records of sunspot numbers and aurorae can be used to estimate sunspot-number maxima from AD 300. Sunspot number maxima from 649 AD to AD 2000 were estimated, one in multiples of 11.1 years and another of ≈ 78 years. The length of a sunspot-number cycle is longer in weak-aurora periods (Shove, 1955). Tables of sunspot numbers have been estimated for 1610 to 1960 (Waldmeier, 1961). Sunspot numbers may arise from a stochastic process (Siscoe, 1976) or from a deterministic chaotic process (Feynman and Gabriel, 1990). Chaotic behavior results from competition between linear instability and nonlinear suppression of cycles (Kremliovski, 1994, 1995). Describing activity cycles with sunspot numbers or group sunspot number gives similar results (Hoyt and Schatten, 1988a, 1988b).

Short periodicities in sunspot numbers of 27, 30, 50, and 150 days have been identified (Torrence and Campo, 1998). Longer-term periodicities of 50 – 80, 90 – 120, and 120 – 260 days may have existed for 10 000 years (Ogurtsov *et al.*, 2002). Hemispheric solar activity is asymmetric with each cycle but approximate 11-year cycles (Li, Yun, and Gu, 2001). There are other proxies for solar activity including sunspot areas, the 10.7-cm radio flux, the solar wind, the cosmogenic isotopes ^{10}Be and ^{14}C, the geomagnetic aa index, solar irradiance, the Mg II index, magnetic flux, aurora, and the flare index (Eddy, 1977).

5. Length of Data Sets

For statistical treatment of the stochastic regime, the length of the data set depends on the persistence and conservation of the time series of the data. Chapman and Bartels (1940) derived the equivalent number of repetitions $[\varepsilon(h)]$ and the effective number of random coordinates, $[h/\varepsilon(h)]$, where m is the standard deviation of the averages of the numbers:

$$\varepsilon(h) = \left[m(h)/(m/\sqrt{h})\right]^2 = hm^2(h)/m^2 \tag{6}$$

and showed that a data set with the length of an activity cycle, about 11 years, has only 20 independent values. This means that to use random statistical methods to analyze data, the set must be very long, much longer than an activity cycle.

The correlation dimension $[D_2]$ is a fractal dimension

$$D_2 = \mathrm{d}\log\left[C(r)\right]/\mathrm{d}\log r, \tag{7}$$

where

$$C(q,r) = r^{(q-1)/Dq}. \tag{8}$$

For $q = 2$, the number of data points $[N]$ needed (Eckman and Ruelle, 1992) is at least

$$2.3\ln N = D_2/2. \tag{9}$$

According to Equation (9) the number of data points to cover the attractor and avoid sample-size problems is about 1000 and a single activity cycle (11 years or 4096 days) has enough points to estimate D_2 and determine whether a cycle is chaotic.

The local Lyapunov exponents are functions of x and L, where L is the total length from each calculation starting point on an attractor where evaluation of the Lyapunov exponents begins. An average over all of these starts yields the average Lyapunov exponents. $L = 1024$ is usually enough (Abarbanel, 1996). Possible effects of sample size are avoided by using

a long time series. There are no precise criteria for determining the size of the data set for calculating the exponents for a particular dynamic system. As a general rule, the number of data points increases with the dimension of the attractor (Brown, Bryant, and Abarbanel, 1991):

$$\log N_{\mathrm{D}} \approx d_{\mathrm{A}}. \tag{10}$$

Equation (10) gives an estimate of the number of data points large enough to cover the attractor and avoid sample-size problems. For $d_{\mathrm{A}} = D_2 \sim D_{\mathrm{L}} = 3$, where D_{L} is the Lyapunov dimension, and $N_{\mathrm{D}} = 1000$, so the number of points in a single cycle is probably high enough to determine the Lyapunov exponents.

6. Nonlinear Analysis of the 10.7-cm Radio Flux for Cycles 19, 20, and 21

This section describes the nonlinear analysis applied to the 10.7-cm radio flux values for Cycles 19, 20, and 21. Appendix B of Greenkorn (2009) describes in detail the calculation algorithms of Abarbanel (1996) and Abarbanel, Frison, and Tsmring (1998). The algorithms are used to calculate the optimum time lag, embedding dimension, local dynamical dimension, the correlation sum and its derivative, and the Lyapunov dimensions.

To convert a time sequence such as Equation (4) to phase space, a time delay must be selected. A prescription for selecting the time delay is the first minimum of the average mutual information *versus* time lag T,

$$I_{AB}(T) = \sum_{ab} P_{AB}(a,b) \log_2\bigl[P_A(a) P_B(b) / P_{AB}(a,b)\bigr], \tag{11}$$

where a is at time k and b is at $k+T$, P_{AB} is the joint probability of A and B, P_A and P_B are the probabilities of A and B. The lowest dimension that unfolds the attractor so that there are no overlaps from projection of the attractor to a lower dimension space is the global embedding dimension.

The stability of motions on the attractor is determined by the Lyapunov exponents defined in Section 2. Dissipation in the dynamical system requires

$$\sum_{a=1}^{d} \lambda_a < 0, \tag{12}$$

so volumes in phase space shrink with time. If one of the λ_a is greater than zero, the dynamical system may be chaotic. If one of the λ_a is zero, the system can be described by a set of ordinary differential equations. Evaluating the average Lyapunov exponents forward and backward gives d_{L} that have the same value but with a sign change. These are the correct exponents. There may be $d_{\mathrm{E}} - d_{\mathrm{L}}$ that do not change sign. If the sum of the exponents is positive the system is probably stochastic.

The Lyapunov dimension $[D_{\mathrm{L}}]$ (Kaplan and Yorke, 1979) can be associated with a volume in phase space that does not change. D_{L} is an estimate of the fractal dimension $[d_{\mathrm{A}}]$ of the system:

$$D_{\mathrm{L}} = K + \sum_{a=1}^{K} \lambda_a / \lambda_{K+1}. \tag{13}$$

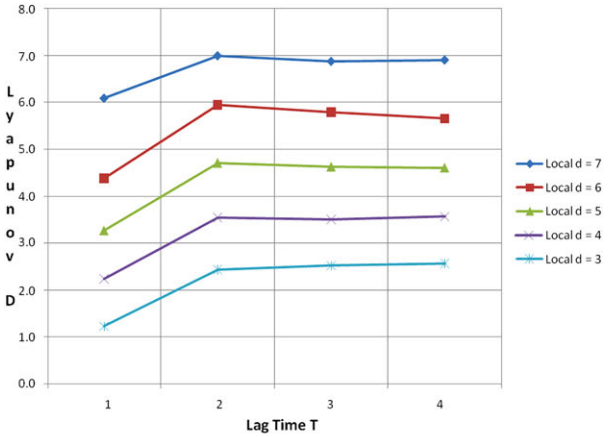

(a)

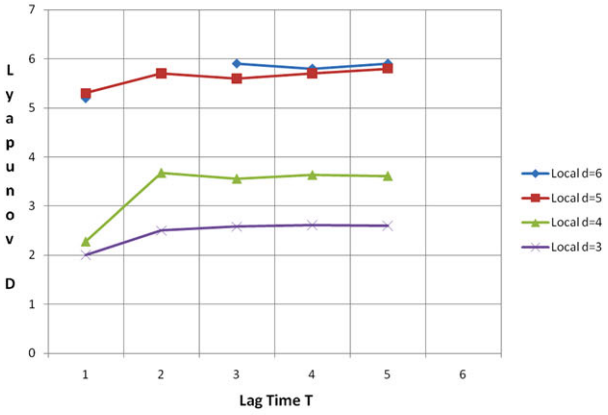

(b)

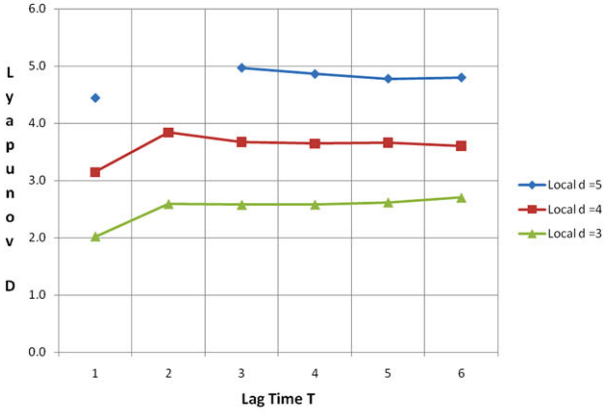

(c)

Figure 1 10.7-cm radio flux values – Lyapunov D_L *versus* lag time T for Cycle 20 with embedding dimension of 7 (a), 6 (b), and 5 (c).

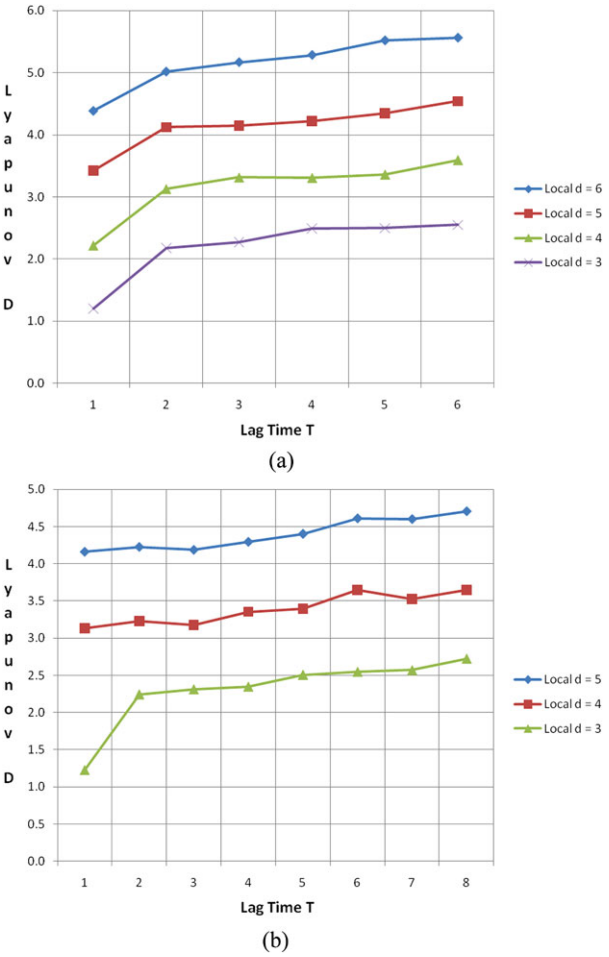

Figure 2 10.7-cm radio flux values – Lyapunov D_L *versus* lag time T for Cycle 21 with embedding dimension of 6 (a) and 5 (b).

7. Discussion

The optimum time delay [T_{OP}], embedding dimension [d_E], local dimension [d_L], Lyapunov dimension [D_L], and the sum of the Lyapunov exponents were calculated for the daily values of the 10.7-cm radio flux for Cycles 19, 20, and 21 using the flux values from the radio flux data in "Solar Variability Affecting Earth" National Oceanic and Atmospheric Administration (NOAA) CD Rom NGDC-05/1. The number of flux values and sunspot numbers used for Cycle 19 is 3872, for Cycle 20 is 4201, and for Cycle 21 is 3761. The Lyapunov exponents are determined by calculating the eigenvalues of the Jacobian matrix of the dynamics. The Lyapunov dimensions are calculated using Equation (13) and the spectrum of Lyapunov exponents. The values of D_L *versus* time lag [T] are plotted in Figure 1 for Cycle 20 for embedding dimensions of 7, 6, and 5. The values of D_L *versus* time lag are plotted in Figure 2 for Cycle 21 for embedding dimensions of 6 and 5. The values of D_L *versus* time lag T are plotted in Figure 3 for the combined values in Cycles 20 and 21 for embedding dimensions of 7 and 6.

In all of these plots, D_L is leveling off at a time lag of four. This value of D_L is the fractal dimension of the attractor.

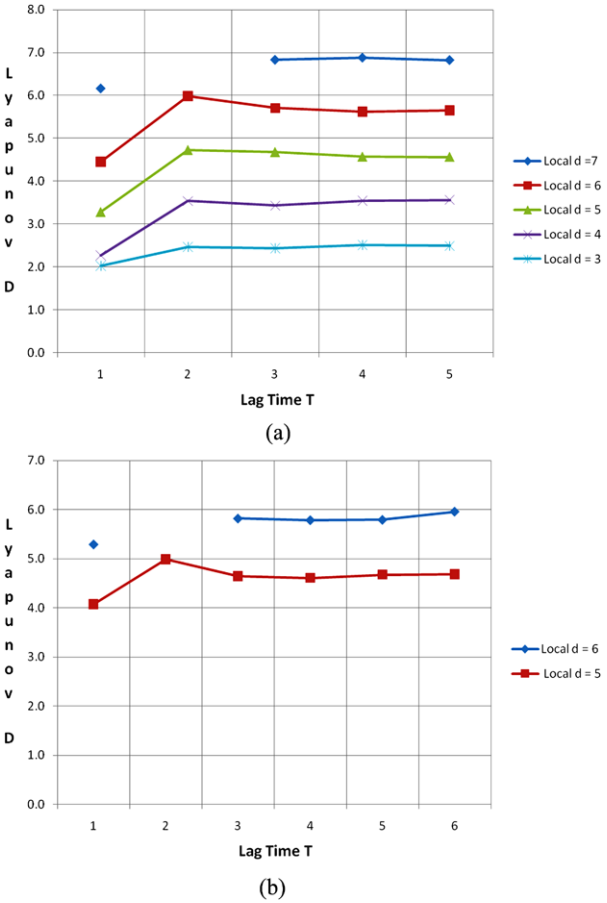

Figure 3 10.7-cm radio flux values – Lyapunov D_L *versus* lag time T for Cycles 20 + 21 with embedding dimension of 7 (a) and 6 (b).

The values of D_L *versus* time lag T for Cycle 20 were determined for embedding dimension 7 and local dimensions 7, 6, 5, 4, and 3; for embedding dimension 6 and local dimensions 6, 5, 4, and 3; for embedding dimension 5 and local dimensions 5, 4, and 3 for the radio flux values and sunspot numbers. Figure 4 is an example of the comparison of the radio flux and the sunspot number for embedding dimensions 7, 6, and 5 and local dimension 5F (radio flux) and 5R (sunspot number) for Cycle 20. Figure 5 is an example of the comparison of the radio flux and the sunspot number for embedding dimensions 7, 6, and 5 and local dimension 5F (radio flux) and 5R (sunspot number) for Cycle 21. The embedding dimension at the optimum time delay was determined by finding the dimension for which the number of false nearest neighbors approaches zero. The local dimension is determined by calculating where the percentage of bad predictions becomes independent of the dimension and number of neighbors.

A day-by-day comparison of the sunspot numbers and the radio-flux values was accomplished as follows. The radio-flux values and the sunspot numbers were each made dimensionless by dividing each value in each cycle by the maximum value in that cycle obtaining $R_i/R_{i\max}$ and $F_{10.7}/F_{10.7\max}$. (The maximum values for R_i and $F_{10.7}$ occurred on the same day for Cycle 20 and one day apart for Cycle 21.) The difference between the dimensionless values of the sunspot numbers and the radio-flux numbers was calculated for each of the

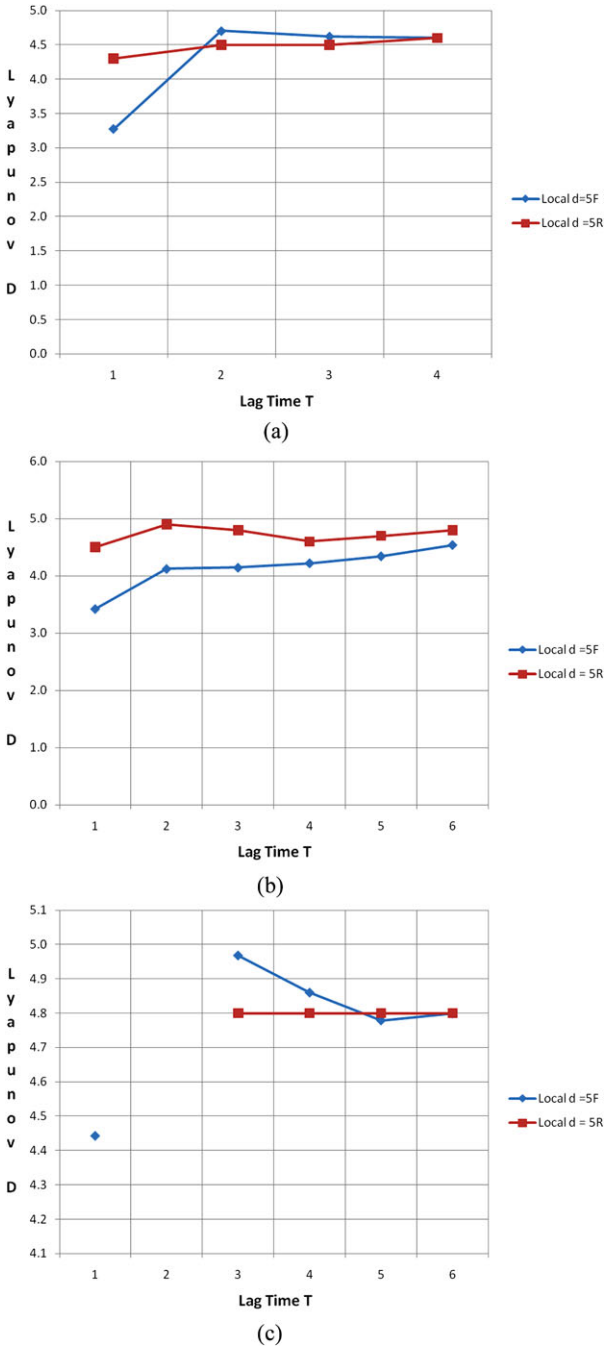

Figure 4 Comparison of 10.7-cm radio flux values [$F_{10.7}$] and International Sunspot Numbers [R_i] for Cycle 20 with embedding dimension of 7 (a), 6 (b), and 5 (c) and local dimension 5F and 5R.

cycles. The differences are plotted *versus* cycle day in Figure 6 for Cycle 19, Figure 7 for Cycle 20, and Figure 8 for Cycle 21 (if the differences were all zero), there would be perfect correspondence.

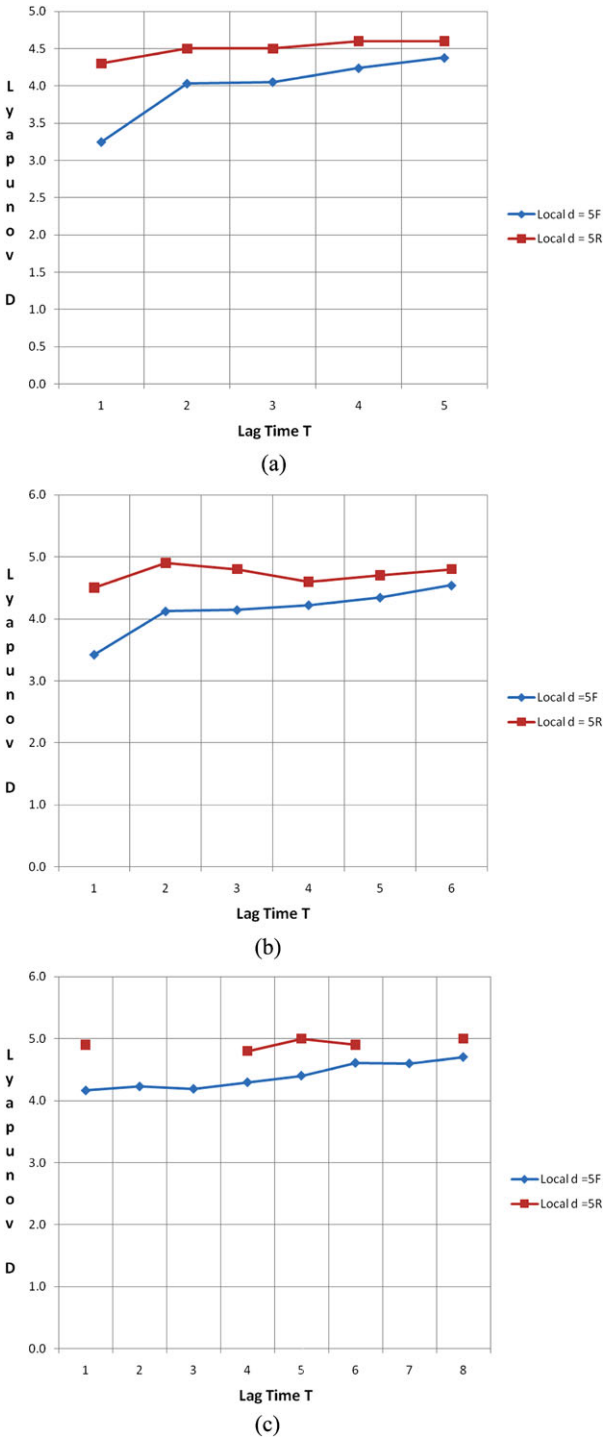

Figure 5 Comparison of 10.7-cm radio flux values [$F_{10.7}$] and International Sunspot Numbers [R_i] for Cycle 21 with embedding dimension of 7 (a), 6 (b), and 5 (c) and local dimension of 5F and 5R.

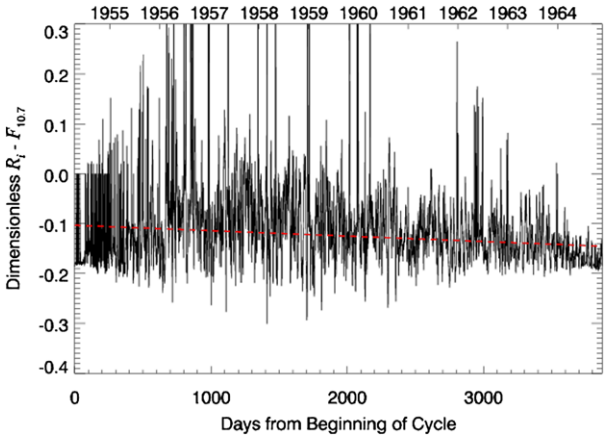

Figure 6 Difference between dimensionless $[R_i]$ and dimensionless $[F_{10.7}]$ for Cycle 19, starting on 20 April 1954.

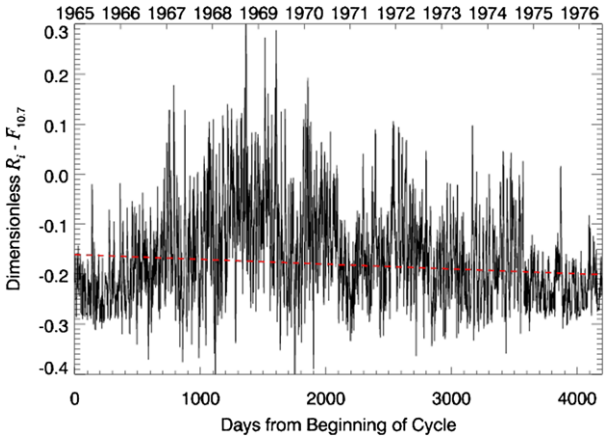

Figure 7 Difference between dimensionless $[R_i]$ and dimensionless $[F_{10.7}]$ for Cycle 20, starting on 1 January 1965.

8. Conclusions

For Cycle 19, the sum of the Lyapunov exponents is positive indicating that the flux values are stochastic. For Cycle 20 there is a positive Lyapunov exponent, the sum of the Lyapunov exponents is negative, and the Lyapunov dimensions are fractal for embedding dimensions 7, 6, and 5 indicating that the flux values are chaotic. For Cycle 21 there is a positive exponent, the sum of the Lyapunov exponents is negative, and the Lyapunov dimensions are fractal for embedding dimensions 6 and 5 indicating that the flux values are chaotic. The embedding dimension at the optimum time delay was determined by finding the dimension for which the number of false nearest neighbors approaches zero. The local dimension is determined by calculating where the percentage of bad predictions becomes independent of the dimension and number of neighbors.

Generally the plots of D_L *versus* T for all combinations are similar to the plots shown in Figures 4 and 5. The two sets (5F and 5R) are parallel with very close values at the maximum time lag. Usually the value for the sunspot number is higher than the radio flux but within 0.2 of the radio flux value. The plots show that the radio flux-values and sunspot numbers are in agreement. The differences in each of Figures 6, 7, and 8 show a trend line with a negative

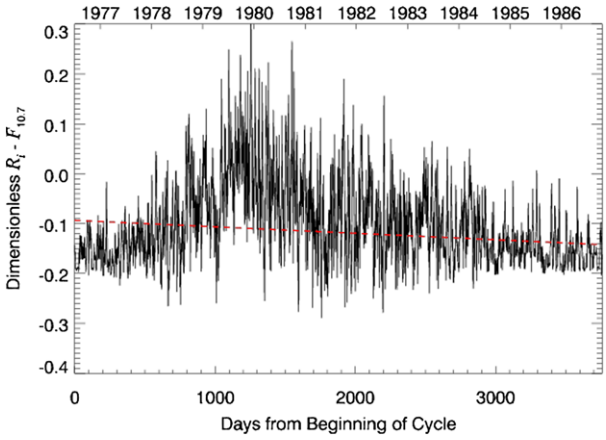

Figure 8 Difference between dimensionless [R_i] and dimensionless [$F_{10.7}$] for Cycle 21, starting on 3 July 1976.

slope, which indicates a more complex relation between the two dimensionless values than if the slope were zero.

The radio-flux values indicate that there is a transition from stochastic to chaotic behavior between Cycles 19 and 20. The sunspot numbers indicated the same transition (Greenkorn, 2009). The radio-flux values seem more consistent showing chaotic behavior than the sunspot numbers. The radio-flux values may be a better indicator of magnetic changes than the sunspot numbers and a more consistent proxy for solar activity. The change in the radio-flux values between Cycles 19 and 20 implies, as did the sunspot numbers, a change in the scale of turbulence in the convection region. The differences in each of Figures 6, 7, and 8 shows a trend line with a negative slope, which indicates a more complex relation between the two dimensionless values than if the slope were zero.

Acknowledgements The values of the International Sunspot number [R_i] are from the Solar Influence Data Centre (SIDC). The values of the 10.7-cm radio flux are from the radio flux data in "Solar Variability Affecting Earth," National Oceanic and Atmospheric Administration (NOAA) CD Rom "NGDC-05/1". Cycle times are from the NOAA/National Geophysical Data Center. Calculation of Lyapunov exponents, optimum time lag, global embedding dimension, local dimension, correlation sum, and dimension D_2 were calculated using cspW a set of algorithms in "Tools For Dynamics" provided by H.D.I. Abarbanel.

References

Abarbanel, H.D.I.: 1996, *Analysis of Observed Chaotic Data*, Springer, New York.
Abarbanel, H.D.I., Frison, T.W., Tsmring, L.S.: 1998, *IEEE Signal Process.* **15**, 49.
Alissandrakis, C.E.: 1997, In: Schmieder, B., del Toro Iniesta, J.C., Vazquez, M. (eds.) *1st Advances in Solar Physics Euroconference*, *Advances in Physics of Sunspots* **CS-118**, Astron. Soc. Pacific, San Francisco, 150.
Bouwer, S.D., Pap, J., Donnelly, R.F.: 1990, In: Schatten, K.H., Arking, A. (eds.) *Climate Impact of Solar Variability* **CP-3086**, NASA, Greenbelt, 125.
Brown, R., Bryant, P., Abarbanel, H.D.I.: 1991, *Phys. Rev. A* **43**, 2787.
Chapman, S., Bartels, J.: 1940, *Geomagnetism*, Clarendon, Oxford, 582.
Chatterjee, T.N., Das, T.K.: 1995, *Mon. Not. Roy. Astron. Soc.* **274**, 858.
Covington, A.E.: 1947, *Nature* **159**, 405.
Covington, A.E.: 1948, *Proc. Inst. Radio Eng.* **36**, 454.
D'Silva, S., Howard, R.F.: 1994, *Solar Phys.* **151**, 213. ADS: http://adsabs.harvard.edu/abs/1994SoPh..151..213D, doi:10.1007/BF00679072.
DeToma, G., White, O.R., Harvey, K.L.: 2000, *Astrophys. J.* **529**, 1101.
Donnelly, R.F.: 1982, *J. Geophys. Res.* **87**, 6331.

Donnelly, R.F.: 1987, *Solar Phys.* **109**, 37. ADS: http://adsabs.harvard.edu/abs/1987SoPh..109...37D, doi:10.1007/BF00167398.
Donnelly, R.F., Heath, D.F., Lean, J.L., Rottman, G.J.: 1983, *J. Geophys. Res.* **88**, 9883.
Eckman, J.P., Ruelle, D.: 1992, *Physica D* **56**, 185.
Eddy, J.A.: 1977, In: White, O.R. (ed.) *The Solar Output and Its Variation*, Colorado Assoc. Univ. Press, Boulder, 51.
Feder, J.: 1989, *Fractals*, Plenum, New York.
Feynman, J., Gabriel, S.B.: 1990, *Solar Phys.* **127**, 393. ADS: http://adsabs.harvard.edu/abs/1990SoPh..127..393F, doi:10.1007/BF00152176.
Foukal, P., Lean, J.: 1990, *Science* **247**, 556.
Grassberger, P., Procaccia, I.: 1983, *Phys. Rev. Lett.* **50**, 346.
Greenkorn, R.A.: 2009, *Solar Phys.* **255**, 301. ADS: http://adsabs.harvard.edu/abs/2009SoPh..255..301G, doi:10.1007/s11207-009-9331-z.
Howard, R.F.: 1984, *Annu. Rev. Astron. Astrophys.* **22**, 131.
Hoyt, D.V., Schatten, K.H.: 1988a, *Solar Phys.* **179**, 189. ADS: http://adsabs.harvard.edu/abs/1998SoPh..179..189H, doi:10.1023/A:1005007527816.
Hoyt, D.V., Schatten, K.H.: 1988b, *Solar Phys.* **181**, 491. ADS: http://adsabs.harvard.edu/abs/1998SoPh..181..491H, doi:10.1023/A:1005056326158.
Kane, R.P., Vats, H.O., Sawant, H.S.: 2001, *Solar Phys.* **201**, 181. ADS: http://adsabs.harvard.edu/abs/2001SoPh..201..181K, doi:10.1023/A:1010349014498.
Kaplan, J., Yorke, I.: 1979, In: Pettegen, H.O., Walther, H.O. (eds.) *Functions and Differential Equations and Approximation of Fixed Points*, Springer, New York.
Kononovich, E.V., Shefov, N.N., Khramova, M.N.: 2002, *Geomagn. Aeron.* **42**(4), 453.
Kremliovski, M.N.: 1994, *Solar Phys.* **151**, 351. ADS: http://adsabs.harvard.edu/abs/1994SoPh..151..351K, doi:10.1007/BF00679081.
Kremliovski, M.N.: 1995, *Solar Phys.* **159**, 371. ADS: http://adsabs.harvard.edu/abs/1995SoPh..159..371K, doi:10.1007/BF00686538.
Li, K.J., Yun, H.S., Gu, X.M.: 2001, *Astrophys. J. Lett.* **554**, L115.
Mouradian, Z., Bocchia, R., Botton, C.: 2002, *Astron. Astrophys.* **394**, 1103.
Ogurtsov, M.G., Nagovitsyn, Yu.A., Kocharov, G.E., Jungner, H.: 2002, *Solar Phys.* **211**, 371.
Oseledec, V.I.: 1968, *Trans. Mosc. Math. Soc.* **19**, 197.
Oster, L.: 1990, *J. Geophys. Res.* **95**, 6247.
Rigozo, N.R., Echer, E., Viera, L.E.A., Nordemann, D.J.R.: 2001, *Solar Phys.* **203**, 179. ADS: http://adsabs.harvard.edu/abs/2001SoPh..203..179R, doi:10.1023/A:1012745612022.
Rogachevskii, I., Kleeorin, N.: 2007, *Phys. Rev. E* **76**, 1.
Rušin, V., Rybansky, M.: 1990, *Bull. Astron. Inst. Czech.* **41**, 263.
Ruzmakin, A.: 2001, *Space Sci. Rev.* **95**, 43.
Salakhutdinova, I.I.: 1998, *Solar Phys.* **181**, 221. ADS: http://adsabs.harvard.edu/abs/1998SoPh..181..221S, doi:10.1023/A:1016555207872.
Salakhutdinova, I.I.: 1999, *Solar Phys.* **188**, 377. ADS: http://adsabs.harvard.edu/abs/1999SoPh..188..377S, doi:10.1023/A:1005265229175.
Schmahl, E.J., Kundu, M.R.: 1998, In: Balasubrarmaniam, K.S., Harvey, J.W., Rabin, D.M. (eds.) **CS-140**, Astron. Soc. Pacific, San Francisco, 387. ADS: http://adsabs.harvard.edu/abs/1998ASPC..140..387S.
Shove, D.J.: 1955, *J. Geophys. Res.* **60**, 127.
Siscoe, G.L.: 1976, *J. Geophys. Res.* **81**, 6224.
Takens, F.: 1980, In: Rand, D., Young, L.S. (eds.) *Dynamical Systems and Turbulence*, Springer, Berlin, 898.
Tapping, K.F., Boteler, D., Charboneau, P., Manson, A., Paquette, H.: 2007, *Solar Phys.* **246**, 309. ADS: http://adsabs.harvard.edu/abs/2007SoPh..246..309T, doi:10.1007/s11207-007-9047-x.
Tapping, K.F., DeTracy, B.: 1990, *Solar Phys.* **127**, 321. ADS: http://adsabs.harvard.edu/abs/1990SoPh..127..321T, doi:10.1007/BF00152171.
Torrence, C., Campo, G.P.: 1998, *Bull. Am. Meteorol. Soc.* **79**, 61.
Ulrich, R., Bertello, L.: 1995, *Nature* **377**, 214.
Waldmeier, M.: 1961, *The Sunspot-Activity in the Years 1610 – 1960*, Schulthess & Co. Ag, Zurich.
Watari, S.: 1995, *Solar Phys.* **158**, 365. ADS: http://adsabs.harvard.edu/abs/1995SoPh..158..365W, doi:10.1007/BF00795669.
Watari, S.: 1996, *Solar Phys.* **163**, 371. ADS: http://adsabs.harvard.edu/abs/1996SoPh..163..371W, doi:10.1007/BF00148008.
White, O.R., Rottman, G.J.: 2000, *Space Sci. Rev.* **94**, 93.
Wilson, R.M., Rabin, D., Moore, R.L.: 1987, *Solar Phys.* **111**, 279. ADS: http://adsabs.harvard.edu/abs/1987SoPh..111..279W, doi:10.1007/BF00148520.
Xanthakis, J., Poulakos, C.: 1985, *Astrophys. Space Sci.* **111**, 179.